MODELING OF THE EVOLUTION OF THE OPTICAL, RADIATIVE, AND THERMODYNAMIC CHARACTERISTICS OF THE ATMOSPHERE DURING CLOUD CRYSTALLIZATION. II. CLOUD FORMATION AFTER DISPERSAL

K.Ya. Kondrat'ev, M.V. Ovchinnikov, V.I. Khvorost'yanov

Institute of Limnology
of the Academy of Sciences of the USSR, Leningrad
and Central Aerological Observatory, Dolgoprudnyĭ
Received November 20, 1989

Numerical experiments on artificial cloud crystallization were performed in order to study the effect of the underlying surface on cloud formation and on the optical properties of the clouds after artificial dispersal. It is shown that repid formation of clouds above moist soil can prevent improvement of the optical parameters of the atmosphere and interfere with controlled modification of the optical weather.

In the Part I of this study[1] we described a numerical experiment in which a supercooled cloud was completed, dispersed by means of artificial crystallization and the optical and radiation characteristics of the lower atmosphere were thereby significant altered. In practice, however, it is by no means always possible to achieve such a strong effect. The clouds can disperse only partially on reform after dispersal. The result of seeding is determined by many parameters, some of the most important of which are the properties of the underlying surface. This part of our study is devoted to the investigation of the effect of the moisture content of the underlying surface on the evolution of the optical, radiation, and meteorological characteristics of the atmosphere during artificial cloud crystallization.

The formation and the initial stage of the evolution of clouds in the case of a moist underlying surface proceed analogously to the case of dry soil presented in the Part I of this study.[1]

Like in the previous variant of the calculation, the seeding started at 7 a.m.. This choice of the moment (soon after sunrise) of seeding is explained by the fact that one goal of the numerical experiment was to estimate the maximum possible perturbations of the meteorological elements resulting from changes produced in the optical properties and radiation regime of the clouds by artificial crystallization and dispersal of the clouds. It is obvious that the perturbations will be all the stronger the longer the Sun shines on the seeded zone. The seeding process consisted of periodic seeding from an aircraft (with a period Δt = 10 min), as described in Part I of this work.[1]

One hour after seeding starts the central part of the cloud crystallizes and stable clearing, extending 20–25 km downwind from the line of seeding occurs (Fig. 1a, to the right of the marker x = 11 km). However, complete dispersal of the clouds does not occur. The obscuring crystalline haze fills practically the entire seeded space, and 30 km from the seeding zone the cloud reforms (Figs. 1a, 1b). One of the determining parameters, which the reformation of the clouds after dispersal depends, is the effective condensation coefficient α_{eff}, which describes the moistening of the soil and appears in the equation of continuity of the vapor flux at the underlying surface[2]:

$$- k_0 \frac{\partial q}{\partial z} = \alpha_{eff} \frac{\bar{V}_w}{4} (q_s - q_0)$$

Here $\bar{V}_w$ is the velocity of the water-vapor molecules; q is the humidity; q_s is the saturating moisture content in the soil; and, q_0 is moisture content at the surface. It is obvious that for $\alpha_{eff} = 0$ $\partial q/\partial z = 0$, which corresponds to no evaporation and condensation on the soil. In this case one can talk about "absolutely dry" soil. If, however, $\alpha_{eff} \sim 1$, then $q \approx q_s$, which corresponds to strongly moistened soil. In the numerical experiment, described in detail in Part I of this work[1] it was assumed that $\alpha_{eff} = 0.1 \cdot 10^{-4}$ ("dry" soil); in the calculations studied in this part of the work it is assumed that $\alpha_{eff} = 0.6 \cdot 10^{-3}$ ("moist" soil).

Figure 2 shows the components of the heat balance underlying surface: the flux of sensible heat B_T; the flux of latent heat B_Q; the heat flux from the soli B_s; and, the radiation balance R_0. Comparing the components of the heat balance for "dry" and "moist" soil shows that redistribution occurs mainly between the sensible heat (B_T) and the latent (B_Q) heat. Evaporation from a dry surface is weak and B_Q does not exceed 10 W/m^2. In this case the flux of sensible heat B_T from the surface into the atmosphere plays the main role in the heat balance: it amounts to at least 150 W/m^2. Such a strong flux results in significant heating of the lower air layers by 8–10°C (these temperature perturbations were described in Part I of this work[1]). In the case of moist soil the increase in the water vapor flux from the surface into the atmosphere results in a strong increase of the latent heat influx (B_Q), which reaches a maximum of 120 W/m^2. At the

0235-6880/90/06 598-07 $02.00

same time the sensible heat flux B_T decreases by 50–100 W/m^2. Thus, in the first case the rate of water vapor flow into the atmosphere is lower than the rate of increase of the temperature and the undersaturation increases, whereas in the second case the opposite picture is observed. In the case of "moist" soil the rate of growth of the absolute moisture content owing to evaporation from the surface is higher than the rate at which the relative moisture content decreases due to the increase in the temperature. This results in a reduction of the deficit of the dew point and to reformation of the clouds, as will be described above.

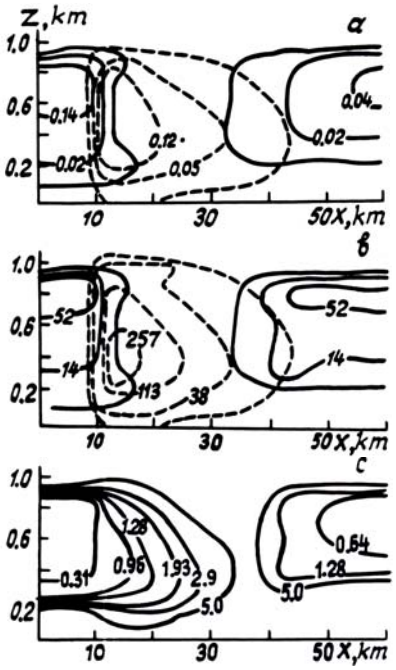

FIG. 1. The two-dimensional fields of the microphysical parameters of the droplet (solid lines) and crystalline (dashed lines) phases and the meteorological visibility 7 hours after seeding starts. q_{L1}, q_{L2}, in g/kg *(a); N_1, in* $10^3 \cdot g^{-1}$, *and N_2, in* g^{-1} *(b); and, L, in* km *(c).*

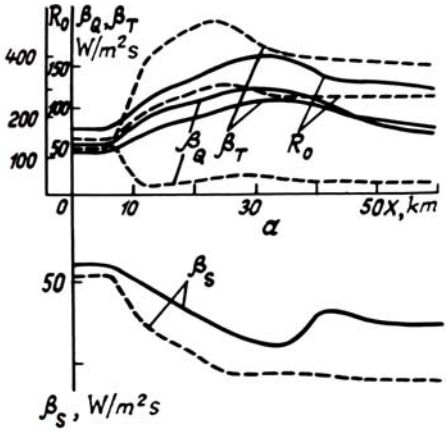

FIG. 2. The components of the heat balance at the surface for dry soil (dashed line) and moist soil (solid lines): the fluxes of sensible heat (B_T), latent heat (B_Q), and heat into the soil (B_s) and the radiation balance (R_0).

In spite of the fact that the concentration of cloud droplets on the left side of the cloud is approximately equal to that on the right side (Fig. 1b), the water content in the flow of the cloud layer (the geostrophic wind oriented along the OX axis and its velocity is 6 m/sec at an altitude of 1.2 km) is 3–3.5 times higher (Fig. 1a). This is explained by the fact that small droplets predominate in the reformed cloud. The same effect is responsible for the relatively low visibility range up to 600 m in this zone (Fig. 1c) while the liquid water content there remains insignificant (up to 0.04 g/kg). When the ice content in the crystallization zone is even higher (from 0.05 to 0.12 g/kg) the meteorological visibility, on the contrary, increases sharply. The visibility range exceeds 1 km in the entire seeded zone, and at a distance of 20 km from the seeding line, as the crystals grow, it reaches approximately 5 km. Thus the crystalline haze with ice content about 0.05 g/kg is practically transparent because of the low concentration and large average size of the particles.

Figure 3 shows the integral characteristics of the solar radiation computed the two-stream approximation:[3,4] the upward ($F_s^{\uparrow}$) and downward ($F_s^{\downarrow}$) fluxes, the influx ($\partial T/\partial t_s$) and the albedo (A). One can see that in the flowing and reforming cloud the upward (Fig. 3a) and downward (Fig. 3b) fluxes of short-wavelength radiation have close values. In the seeding zone itself these fluxes transform significantly. Thus, the downward flux in the cleared zone at an altitude of 200 m ($F_s^{\downarrow}$ = 670 W/m^2) more than two times larger than the flux below the cloud ($F_s^{\downarrow}$ = 319 W/m^2 (Fig. 3b). Because the upward fluxes in both zones are nearly equal at the surface (230 and 200 W/m^2, respectively) the radiation balance of the surface R_0 changes. Twenty kilometers downwind from the seeding line R_0 increases by more than 200 W/m^2 (Fig. 2). This results in heating of the underlying surface, which will be described below.

The formed fine-droplet cloud has, despite its rather low liquid water content (no higher than 0.04 g/kg), a quite high albedo A = 51% (Fig. 3d); in addition, the albedo of the cloud itself $A_c = A - A_{sf}$ constituting 16% (here A_{sf} = 35% is the albedo of the underlying surface). In the flowing cloud layer (A = 64%), i.e., it is less than two times greater than the albedo of the reformed cloud, even though its water content (in the flow q_L = 0.14 g/kg) is 3.5 times higher (Fig. 1a). This comparison shows that size of the cloud particles determines the albedo; this was already pointed at in Refs. 4 and 6. In the central part of the seeded zone, where the cloud has totally crystallized, the albedo is completely insignificant and constitutes only 38%. In addition, the ice content in this zone reaches 0.05 g/kg, i.e., the total water content here is even somewhat higher than in the formed cloud layer (Fig. 1a). The reason is that the crystals propagating downstream, are

continuously growing and their average size in the zone considered (10–20 km from the seeding line) is about 60 μm. As shown in Refs. 3 and 4 a cloud with such a microstructure virtually does not reflect solar radiation with short wavelengths.

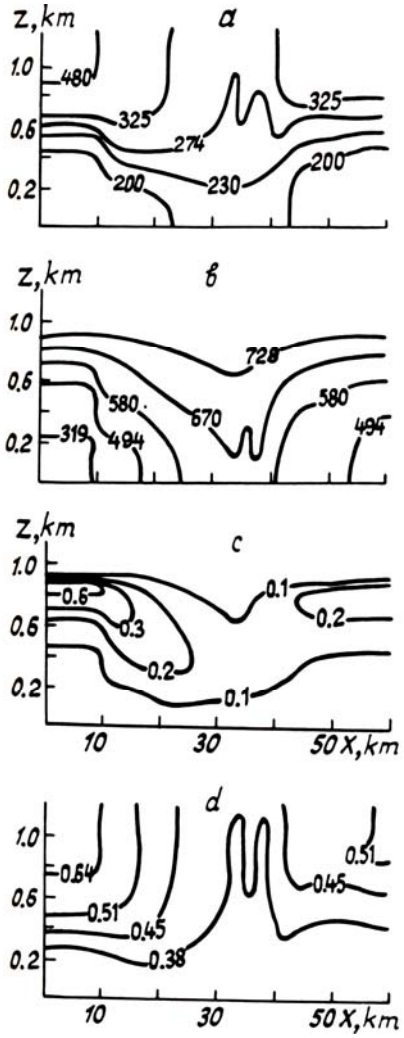

FIG. 3. Vertical section of the fields of the solar radiation parameters: the upward ($F_s^{\uparrow}$, a) and downward ($F_s^{\downarrow}$, b) fluxes, in W/m^2*, the influx of solar radiation* $(dT/dt)_s$*, in* °C/hr *(c), and the albedo (A).*

What we have said above is most vividly illustrated by the vertical profiles of the liquid water and ice content (q_{L1}), the average size of cloud particles ($\bar{r}_1$), the mass spectral scattering coefficient ($\sigma_{\lambda 1}$) at $\lambda = 0.05$ μm wavelength, and the integrated albedo (A), which are all given in Table I. It is obvious that the scattering coefficient increases as the particle size $\bar{r}_1$ decreases. As noted in Refs. 3 and 4 $\sigma_{\lambda 1} \sim \bar{r}_1^{-1}$. The integral albedo of the cloud formed in the entire thickness of the layer increases most in the layers where the comparatively small water droplets or ice crystals are concentrated.

Thus, the main contribution to the total albedo is made by the layer 240–560 m located at the bottom of the cloud, where the average size of the crystals does not exceed 50 μm. The increment to the albedo in this layer is 8% and the increment in the entire cloud is 10%. We emphasize that such weak reflection of solar radiation is observed despite the fact that the total ice content

$$m_2 = \int_{z_B}^{z_T} q_{L2}\, dz$$

is equal to 82.7 g/m^2, i.e., it is almost 7 times greater than the liquid water content of the formed cloud ($x = 54$ km, $m_1 = 12$ g/m^2) and its albedo is somewhat smaller ($A = 45\%$ at $X = 18$ km as compared to $A = 47\%$, $X = 54$ km).

It is evident from Fig. 3c that the heat influx in the crystallized cloud does not exceed 0.1°C/hr, and the flux of solar radiation is notweakened significantly. It can thus be concluded that the seeded zone is practically transparent to short-wavelength radiation.

This is not the case for long-wavelength radiation, and here seeding does not change as strongly either the downward or upward fluxes. The crystalline haze filling the seeded zone is sufficient to screen significantly the effective radiation from the surface, and this contributes to the development of the greenhouse effect.

The temporal evolution of the temperature at the ground for the cases of "moist" (with cloud formation) and "dry" (complete dispersal) soils is presented in Fig. 4. We shall examine first the variant described in detail in this part of the paper (moist soil and reformation of the dispersed cloud occurs). At the start of seeding at 7 a.m. the temperature field is uniform in the horizontal direction (Fig. 4a). But already after two hours the perturbation of the temperature at the ground reaches a maximum 20–25 km from the seeding line. The temperature here is then 2°C higher than beneath the cloud. The temperature continues to increase and by 13:00 LT the perturbation is maximum and equals 4°C. At that moment the minimum temperature at the ground is 4°C (under the cloud) and the maximum temperature is 8°C (in the seeded zone). Reaching a maximum 24 km from the seeding line the temperature starts to decrease (as x increases). This is connected with the fact that the reformed cloud screens the solar radiation flux to the surface. In this case the perturbation virtually does not propagate vertically, and at a height of 200–300 m uniformity in the horizontal plane is observed. After 13:00 LT the temperature starts to drop and one hour after sunset (at 19:00 LT) it evens out at the surface. The diurnal amplitude of the temperature variation in the cloud-covered zone is equal to 5°C, while in the seeded zone it is two times larger.

TABLE I.

Vertical profiles of the liquid water content (q_{L1}) Ice content average size of cloud particles ($\overline{r_1 r_2}$), the bulk spectral scattering coefficient ($\sigma_{\lambda,1}$) at the vawelength $\lambda = 0.5$ μm and the integrated albedo (A) for several values of the horizontal coordinate (x) with indication of the total water content (m_1) (see Fig. 1)

Characteristics	Height, m				
	240	400	560	720	800
$x = 6$ km, $m_1 = 60.2$ g/m^2 (droplet cloud)					
q_{L1}, g/kg	0.004	0.056	0.087	0.105	0.100
$\bar{r}_1$, μm	7.1	6.8	6.2	5.4	4.4
$\sigma_{0.5;1}$, cm^2/g	1633	1707	1883	2151	2638
A, %	35	41	50	58	64
$x = 18$ km, $m_2 = 82.7$ g/m^2 (crystalline cloud)					
q_{L1}, g/kg	0.070	0.139	0.124	0.085	0.030
$\bar{r}_1$, μm	51.9	48.9	49.3	52.5	59.7
$\sigma_{0.5;1}$, cm^2/g	324	344	341	320	282
A, %	35	39	43	45	45
$x = 54$ km, $m_1 = 12.0$ g/m^2 (droplet cloud)					
q_{L1}, g/kg	—	0.016	0.023	0.024	0.016
$\bar{r}_1$, μm	—	5.5	5.2	4.3	2.8
$\sigma_{0.5;1}$, cm^2/g	—	2139	2264	2724	4194
A, %	35	36	39	43	47

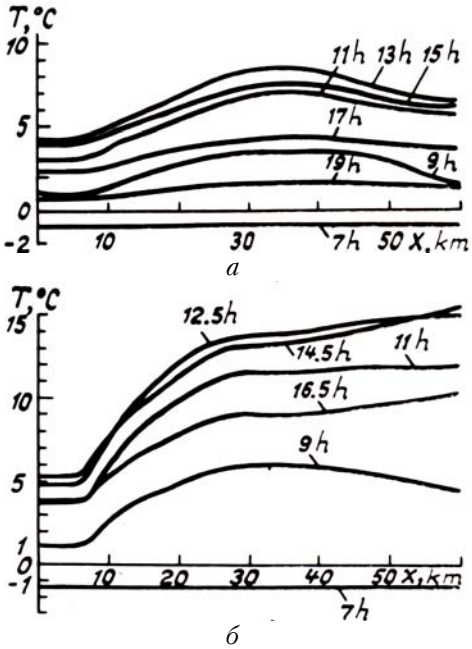

FIG. 4. The temporal evolution of the temperature near the ground for "moist" (a) and "dry" (b) soil.

In the case of dry soil the screening effect of the clouds is not restored and for this reason the perturbation of the temperature is larger. This variant of the calculation is described in detail in Part I of this work.[1] The temporal evolution of the temperature beneath the cloud is close to that described in Ref. 1. The maximum temperature in the dispersal zone is 14°C (Fig. 4b). The temperature contrast is about 9°C. Such a sharp increase in the temperature occurs on a relatively short horizontal section 15–20 km long.

The calculations performed show that artificial crystallization of clouds results in significant transformation of the fields of radiation parameters in the atmospheric boundary layer. However it is not always possible to bring about a qualitative change in the optical weather and complete cloud dispersal. The properties of the underlying surface play a determining role here. The numerical experiments confirmed the importance of separating the liquid and crystal phases in clouds in such models because of the fundamental differences between their optical and radiation characteristics.

The result obtained in this paper should be taken into account when planning and conducting

artificial dispersal of clouds for the purpose of providing favorable operating conditions for different optical systems as well as for forecasting the optical weather.[5]

REFERENCES

1. K.Ya. Kondrat'ev, M.V. Ovchinnikov, and V.I. Khvorost'yanov. Opt. Atmos. **3**, No. 6, 647–654 (1990).
2. G.T. Marchuk, K.Ya. Kondrat'ev, V.V. Kozoderov, and V.I. Khvorost'yanov, *Clouds and Climate* [in Russian], Gidrometeoizdat, Leningrad (1986) 512 pp.
3. K.Ya. Kondrat'ev, M.V. Ovchinnikov, and V.I. Khvorost'yanov. Dokl. Akad. Nauk SSSR **302**, No. 3, 583–587 (1988).
4. K.Ya. Kondrat'ev, M.V. Ovchinnikov, and V.I. Khvorost'yanov, Opt. Atmos. **1**, No. 6, 57–66, No. 7, 98–105 (1988).
5. B.D. Belan and G.O. Zadde, *Forecasting and Monitoring of the Optical and Meteorological State of the Atmosphere* [in Russian), Tomsk Affiliate of the Siberian Branch of the Academy of Sciences of the USSR. Tomsk (1982), pp. 4–20.
6. K.Ya. Kondrat'ev, V.I. Khvorost'yanov, and M.V. Ovchinnikov, in: *Proceeding of the 10-th International Symposium on Atmospheric Radiation,* Lille, France, (1988) pp. 71–72.